Joint Design of Unimodular Waveform and Mismatched Filter Against Interrupted-Sampling Repeater Jamming via Bi-Objective Optimization

Xiaohan Zhao, Yongzhe Li, and Ran Tao
School of Information and Electronics, Beijing Institute of Technology, Beijing 100081, China
Emails: xiaohanzhao@bit.edu.cn, lyz@ieee.org/yongzhe.li@bit.edu.cn, rantao@bit.edu.cn

***Abstract*—This paper focuses on the joint design of unimodular waveforms and mismatched filters to enhance target detection performance and mitigate interrupted-sampling repeater jamming (ISRJ) through a bi-objective optimization framework. The design aims to achieve favorable correlation properties and control the signal-to-noise ratio loss (SNRL) at the mismatched filter output, while concurrently suppressing both the range processing gain and the ISRJ energy. To evaluate target detection performance, we employ a weighted sum of the integrated sidelobe level (ISL) and an SNRL-related penalty term as the primary metric. Meanwhile, jamming suppression is evaluated by the weighted sum of the jamming integrated level and the jamming peak level. Using these multiple metrics, we formulate the design into a non-convex bi-objective optimization problem with unimodular constraints and energy restrictions. To solve it, we propose an algorithm based on the weighted objectives approach, wherein multiple objectives are reformulated into a single objective function with adaptively determined weighting coefficients. The proposed algorithm dynamically updates the weighting coefficients and obtains a closed-form solution via a multiple-gradient descent-based approach that is followed by projections toward the respective feasibility set at each iteration. Simulations verify the effectiveness of the proposed algorithm.**

***Index Terms*—Anti-jamming, interrupted-sampling repeater jamming (ISRJ), correlation levels, bi-objective optimization**

I. Introduction

Jamming suppression has consistently drawn attention over decades [1]–[4], which has developed with the emergence of electronic jamming. In complex electromagnetic environment, electronic jamming is becoming more complicated and poses a threat to the real target detection of radar. With the development of jammer, some electronic jamming, i.e., active deception jamming based on digital radio frequency memory, leads to high false-target peak with low transmitting power. Among active deception jamming, ISRJ has been commonly used due to the advantages of it, such as short response time, high echo similarity, and simple implementation [5]. The countermeasure for ISRJ needs to be further developed.

In light of improving radar detection performances in jamming scenarios, there already exist works on suppressing the ISRJ [6]–[8] using different characteristics between the ISRJ and the true target in time-frequency domain. Earlier works identify jamming and estimate its parameters [8] to design a frequency filter to suppress ISRJ using signal processing methods, i.e., fractional Fourier transform (FrFT) [6], short-time Fourier transform (STFT) [7], etc. However, the capability of ISRJ rejection performance of this kind of methods is limited by the accuracy of ISRJ parameter estimation. The recent work addressing this challenge is presented in [9]–[12], where the authors design waveforms and its corresponding mismatched filter to suppress ISRJ. Most of them aim to obtain good radar detection and anti-jamming performance by optimizing multiple criteria [9]–[11]. Technically, they directly use the sum of the criteria with constant coefficients as the metric of the waveform design problem. However, such joint design considering the bi-objective optimization of these multiple criteria has not been studied in existing literature.

In this paper, we jointly design unimodular waveforms and mismatched filters to obtain good target detection performance and counteract ISRJ. We aim to achieve good correlation properties and control signal-to-noise ratio loss (SNRL) of the mismatched filter output, while simultaneously suppressing the range processing gain and energy of the ISRJ. To this end, we employ a weighted sum of the integrated sidelobe level (ISL) and an SNRL-related penalty term as the primary metric for evaluating target detection performance. For jamming suppression, we adopt the weighted sum of the jamming integrated level and jamming peak level as the key metric. Then, we formulate the design into a non-convex bi-objective optimization problem with unimodular constraints and energy restrictions. To solve it, we propose an algorithm based on weighted objectives approach, wherein the multiple objectives are reformulated into a single weighted objective function. This method involves dynamically updating adaptive weighting coefficients iteratively and solving the reformulated problem via a multiple-gradient descent based method. Then, we conduct projections toward the formulated constraints. Simulations verify the effectiveness of the proposed algorithm.

Notations: We use $(\cdot)^*$, $(\cdot)^{\mathrm{T}}$, $(\cdot)^{\mathrm{H}}$, $(\cdot)^{\dagger}$, $\odot$, $\otimes$ $|\cdot|$, $\|\cdot\|$, ∇, and $[\cdot]_{i,j}$ to denote conjugate, transpose, conjugate transpose, pseudo-inverse, Hadamard product, Kronecker product, modulus, Euclidean norm, gradient, and the (i,j)-th element of a matrix, respectively. Moreover $\mathbf{0}_M$ and $\mathbf{1}_M$ are the $M \times 1$ vectors with all elements being 0 and 1, respectively.

II. Signal model and Problem formulation

Consider a radar system which emits M pulses of unimodular and mutually orthogonal waveforms in a coherent processing interval, each of which has a code length

This work was supported in part by the National Natural Science Foundation of China (NSFC) under grants 62271054 and U21A20456.

equal to L. We denote the waveform vector by $\mathbf{x} \triangleq [\mathbf{x}_1^{\mathrm{T}}, \cdots, \mathbf{x}_M^{\mathrm{T}}]^{\mathrm{T}} \in \mathbb{C}^{LM\times 1}$, whose m-th component corresponds to the m-th launched waveform characterized by $\mathbf{x}_m \triangleq [\mathbf{x}_m(1), \cdots, \mathbf{x}_m(L)]^{\mathrm{T}} \in \mathbb{C}^{L\times 1}$. Let the p-th element of $\mathbf{x}_m$ be $\mathbf{x}_m(p) = e^{j\boldsymbol{\theta}_m(p)}$ where $\boldsymbol{\theta}_m(p)$ is an arbitrary phase value ranging between $-\pi$ and π.

Without loss of generality, the ISRJ signal can be regarded as the partially sampled version of the transmitted waveforms with independent receiving and transmitting channels whose jamming parameters are different. To express the sampling pattern for generating ISRJ, we introduce the interrupted-sampling function as

$$s(t) = \mathrm{rect}(\tfrac{t}{\tau}) \otimes \sum_{n=0}^{+\infty} \delta(t - nT) \tag{1}$$

where $\mathrm{rect}(\cdot)$ is a rectangular window function, τ represents the ISRJ sampling duration, and T is repetition interval of sampling. By discretizing $s(t)$ over the time interval T with an appropriate sampling rate f_s and storing all the obtained samples into a vector denoted by $\mathbf{s} = [s(t)|_{t=1/f_s}, \cdots, s(t)|_{t=L/f_s}]^{\mathrm{T}}$, the ISRJ signal can be written as

$$\mathbf{q}_m = \mathbf{x}_m \odot \mathbf{s}. \tag{2}$$

To suppress the range processing gain of ISRJ signal, the mismatched filter with the weight vector $\mathbf{h}_m \in \mathbb{C}^{L\times 1}$ is applied to the received signal containing the echoes of $\mathbf{x}_m$ and $\mathbf{q}_m$. For later use, we store all the weight vectors $\{\mathbf{h}_m\}_{m=1}^M$ into an vector $\mathbf{h} \triangleq [\mathbf{h}_1^{\mathrm{T}}, \cdots, \mathbf{h}_M^{\mathrm{T}}]^{\mathrm{T}} \in \mathbb{C}^{LM\times 1}$.

From the radar perspective, the output of mismatched filter is expected to have good correlation properties, which ensures the accurate extraction of real targets with the interference of ISRJ jamming. Toward this end, the ISL metric that characterizes the auto-correlations of transmitted waveform in each pulse and its corresponding mismatched filter are typically considered, whose expression is given by

$$\xi_1 \triangleq \sum_{m=1}^{M} \sum_{\substack{l=1-L \\ l\neq 0}}^{L-1} \left|\mathbf{x}_m^{\mathrm{H}} \mathbf{S}_l \mathbf{h}_m\right|^2 \tag{3}$$

where $[\mathbf{S}_l]_{i,j} \triangleq \begin{cases} 1, & j-i=k \\ 0, & \text{else} \end{cases}$. However, the use of the mismatched filter scheme causes the SNRL at the receiver, which is expected to be controlled in a reasonable range. The SNRL of $\mathbf{x}_m$ and $\mathbf{h}_m$ is expressed as $10\mathrm{lg}10\frac{\|\mathbf{x}_m\|^2\|\mathbf{h}_m\|^2}{|\mathbf{x}_m^{\mathrm{H}}\mathbf{h}_m|^2}$. By limiting the energy of mismatched filter by $\|\mathbf{h}_m\|^2 = \tilde{L}$ and using the fact that $\|\mathbf{x}_m\|^2 = L$, the SNRL of $\{\mathbf{x}_m\}_{m=1}^M$ and $\{\mathbf{h}_m\}_{m=1}^M$ can be controlled by minimizing the following function with penalty form

$$\xi_{\mathrm{SNRL}} = \sum_{m=1}^{M} |\mathbf{x}_m^{\mathrm{H}}\mathbf{h}_m - c_1|^2 \tag{4}$$

where c_1 denotes a preset constant. By introducing the weighted coefficient γ_1, the objective function for minimizing the ISL of correlation between transmitted waveforms and mismatched filter and simultaneously controlling the SNRL is expressed as

$$f_1 = \sum_{m=1}^{M} \sum_{\substack{l=1-L \\ l\neq 0}}^{L-1} \left|\mathbf{x}_m^{\mathrm{H}} \mathbf{S}_l \mathbf{h}_m\right|^2 + \gamma_1 \sum_{m=1}^{M} |\mathbf{x}_m^{\mathrm{H}}\mathbf{h}_m - c_1|^2 \tag{5}$$

For the task of jamming suppression, receiving filter should have good orthogonality with the ISRJ signal. Therefore, the sidelobe energy of the correlation between the mismatched filter and ISRJ signal is expected as low as possible. The accumulation of sidelobe energy of correlation between $\mathbf{h}_m$ and $\mathbf{q}_m$ is defined as

$$\xi_2 \triangleq \sum_{m=1}^{M} \sum_{l=1-L}^{L-1} \left|\mathbf{q}_m^{\mathrm{H}} \mathbf{S}_l \mathbf{h}_m\right|^2. \tag{6}$$

Meanwhile, the jamming peak level is also expected to be controlled, which is related to the correlation function of the ISRJ signal and the receiving filter at lag 0. To this end, the following penalty function is introduced

$$\xi_{\mathrm{JPL}} = \sum_{m=1}^{M} |\mathbf{q}_m^{\mathrm{H}}\mathbf{h}_m - c_2|^2 \tag{7}$$

where c_2 is a preset constant used for limiting the jamming peak level. Combining (6) and (7), the objective function for anti-jamming can be expressed as

$$f_2 = \sum_{m=1}^{M} \sum_{\substack{l=1-L \\ l\neq 0}}^{L-1} \left|\mathbf{q}_m^{\mathrm{H}} \mathbf{S}_l \mathbf{h}_m\right|^2 + \gamma_2 \sum_{m=1}^{M} |\mathbf{q}_m^{\mathrm{H}}\mathbf{h}_m - c_2|^2 \tag{8}$$

with γ_2 being a weighted coefficient.

The problem considered here is the joint design of unimodular waveform(s) and mismatched filter, whose objective is to minimize (5) and (8) simultaneously. The above joint design can be written as the following bi-objective problem

$$\begin{aligned} \min_{\mathbf{h},\,\mathbf{x}} \quad & f \triangleq (f_1, f_2) \\ \text{s.t.} \quad & \|\mathbf{h}_m\|^2 = \tilde{L},\ m = 1, \cdots, M \\ & |\mathbf{x}_m(l)| = 1,\ l = 1, \cdots, L,\ m = 1, \cdots, M. \end{aligned} \tag{9}$$

where the first constraint restricts the power of weight vectors to a constant, and the second constraint corresponds to the constant modulus of waveform elements.

III. Joint design of waveforms and mismatched filter for ISRJ suppression

To solve (9), we reformulate f_1 and f_2 as the functions with respect to $\mathbf{w} \triangleq [\mathbf{x}^{\mathrm{T}}, \mathbf{h}^{\mathrm{T}}]^{\mathrm{T}} \in \mathbb{C}^{2LM\times 1}$, which are denoted by $f_1(\mathbf{w})$ and $f_2(\mathbf{w})$, respectively. Introducing $\mathcal{M} \triangleq \{1, \cdots, M\}$ and $\mathbf{U}_p \triangleq [\mathbf{0}_{L\times L(p-1)}, \mathbf{1}_{L\times L}, \mathbf{0}_{L\times L(2M-p)}] \in \mathbb{Z}^{L\times 2LM}$, $p \in [1, 2M]$, we can rewrite f_1 given by (5) as

$$\begin{aligned} f_1(\mathbf{w}) = & \sum_{m=1}^{M} \sum_{\substack{l=1-L \\ l\neq 0}}^{L-1} \left|\mathbf{w}^{\mathrm{H}}\mathbf{U}_m^{\mathrm{H}}\mathbf{S}_l\mathbf{U}_{m+M}\mathbf{w}\right|^2 \\ & + \gamma_1 \sum_{m=1}^{M} |\mathbf{w}^{\mathrm{H}}\mathbf{U}_m^{\mathrm{H}}\mathbf{U}_{m+M}\mathbf{w} - c_1|^2 \end{aligned} \tag{10}$$

which is obtained by substituting $\mathbf{x}_m = \mathbf{U}_m\mathbf{w}, \forall m \in \mathcal{M}$ and $\mathbf{h}_m = \mathbf{U}_{m+M}\mathbf{w}, \forall m \in \mathcal{M}$ into (5). Moreover, resorting to the same routine and using (2), we express f_2 given by (8) as

$$f_2(\mathbf{w}) = \sum_{m=1}^{M}\sum_{l=1-L}^{L-1}\left|(\mathbf{U}_m\mathbf{w}\odot\mathbf{s})^{\mathrm{H}}\mathbf{S}_l\mathbf{U}_{m+M}\mathbf{w}\right|^2 + \gamma_2\sum_{m=1}^{M}\left|(\mathbf{U}_m\mathbf{w}\odot\mathbf{s})^{\mathrm{H}}\mathbf{U}_{m+M}\mathbf{w} - c_2\right|^2. \quad (11)$$

Based on (10) and (11), the bi-objective problem (9) can be expressed as [1]

$$\begin{aligned}\min_{\mathbf{w}} \quad & f(\mathbf{w}) = (f_1(\mathbf{w}), f_2(\mathbf{w}))\\ \text{s.t.} \quad & \|\mathbf{U}_{M+m}\mathbf{w}\|^2 = \tilde{L},\ m \in \mathcal{M}\\ & |\mathbf{U}_m\mathbf{w}| = \mathbf{1}_L,\ m \in \mathcal{M}\end{aligned} \quad (12)$$

where we use $f(\mathbf{w})$ to re-express f for emphasizing on its functionality with respect to $\mathbf{w}$.

Considering that problem (12) is bi-objective, we aim to find solutions that improve one objective without degrading the other. To solve (12), we propose an algorithm based on the weighted objectives method with adaptive weighting coefficients to ensure simultaneous reduction of all objectives. The adaptive weighting coefficients are dynamically adjusted at each iteration to guide the variables towards a Pareto or weakly Pareto optimal solution [13]. The details of the proposed algorithm are shown as follows.

We reformulate the objective function of (12) as the weighted sum of f_1 and f_2, using adaptive coefficients to guide the variable updates toward a Pareto or weakly Pareto optimal solution [13]. The coefficients are dynamically adjusted at each iteration by solving a quadratic problem with a given $\mathbf{w}$. Then, we minimize the aggregated objective function via a multiple-gradient [14] descent based approach and leverage to projection towards the constraints of (12) at each iteration. In the following, we present our detailed solution to (12).

A. Problem Reformulation and Coefficients Determination

By introducing the adaptive coefficient vector $\boldsymbol{\alpha} \triangleq [\alpha_1, \alpha_2]^{\mathrm{T}} \in \mathbb{R}^{2\times 1}$ with $\mathbf{1}_2^{\mathrm{T}}\boldsymbol{\alpha} = 1$, we transform (12) as follows

$$\begin{aligned}\min_{\mathbf{w}} \quad & \tilde{f}(\mathbf{w}) \triangleq \sum_{i=1}^{2}\alpha_i f_i(\mathbf{w})\\ \text{s.t.} \quad & \|\mathbf{U}_{M+m}\mathbf{w}\|^2 = \tilde{L},\ m \in \mathcal{M}\\ & |\mathbf{U}_m\mathbf{w}| = \mathbf{1}_L,\ m \in \mathcal{M}.\end{aligned} \quad (13)$$

Before proceeding with (13), we need to determine $\boldsymbol{\alpha}$. To this end we present the following lemma.

Lemma 1. *Let $\mathbf{w}^*$ be a Pareto optimal solution of the problem* (13)*. Then, there exists non-negative scalars $\alpha_1 > 0$ and $\alpha_2 > 0$ such as $\sum_{i=1}^{2}\alpha_i = 1$ and $\sum_{i=1}^{2}\alpha_i\nabla f_i(\mathbf{w}) = 0$.*

Proof. See the proof in [15] □

[1]Here, the modulus function $|\cdot|$ is applied to a vector argument, whose calculation is conducted in terms of each element of the input vector.

Applying Lemma 1, we consider the following quadratic problem for a given $\mathbf{w}$ at each iteration

$$\begin{aligned}\min_{\boldsymbol{\alpha}} \quad & \|\sum_{i=1}^{2}\alpha_i\nabla f_i(\mathbf{w})\|^2\\ \text{s.t.} \quad & \mathbf{1}_2^{\mathrm{T}}\boldsymbol{\alpha} = 1\\ & \mathbf{1}_2 \succeq \boldsymbol{\alpha} \succeq \mathbf{0}_2\end{aligned} \quad (14)$$

whose solution is the desired adaptive coefficient vector $\boldsymbol{\alpha}$. To solve (14), we first tackle the problem with all the other constraints omitted except the equality constraint, given by

$$\min_{\tilde{\boldsymbol{\alpha}}} \ \|\sum_{i=1}^{2}\tilde{\alpha}_i\nabla f_i(\mathbf{w})\|^2 \quad \text{s.t.} \ \mathbf{1}_2^{\mathrm{T}}\tilde{\boldsymbol{\alpha}} = 1 \quad (15)$$

with $\tilde{\boldsymbol{\alpha}} \triangleq [\tilde{\alpha}_1, \tilde{\alpha}_2]^{\mathrm{T}} \in \mathbb{R}^{2\times 1}$ being the vector containing the solutions to (15). By using the Lagrange multiplier method, the solution to (15) at the k-th iteration can be calculated by

$$\tilde{\boldsymbol{\alpha}}^{(k)} = \mathbf{E}(\mathbf{W}^{(k-1)})^{\dagger}\mathbf{e}_3 \quad (16)$$

whose details are omitted to show because of the space limitation. Herein, $\mathbf{E} \triangleq [\mathbf{e}_1, \mathbf{e}_2]^{\mathrm{T}} \in \mathbb{R}^{2\times 3}$ with $\mathbf{e}_i \in \mathbb{R}^{3\times 1}$ being a vector composed of all zeros except the i-th element equaling 1, $\mathbf{W}^{(k-1)} \triangleq \begin{bmatrix} 2\hat{\mathbf{W}}^{(k-1)}(\hat{\mathbf{W}}^{(k-1)})^{\mathrm{H}} & \mathbf{1}_2 \\ \mathbf{1}_2^{\mathrm{T}} & 0 \end{bmatrix} \in \mathbb{C}^{3\times 3}$, $\hat{\mathbf{W}}^{(k-1)} \triangleq [\nabla f_1(\mathbf{w})|_{\mathbf{w}=\mathbf{w}^{(k-1)}}, \nabla f_2(\mathbf{w})|_{\mathbf{w}=\mathbf{w}^{(k-1)}}]^{\mathrm{H}} \in \mathbb{C}^{2\times L}$, $\mathbf{w}^{(k-1)}$ denotes the vector obtained at the $(k-1)$-th iteration, and $\nabla f_i(\mathbf{w})|_{\mathbf{w}=\mathbf{w}^{(k-1)}}$ is the gradient of $f_i(\mathbf{w})$ at $\mathbf{w}^{(k-1)}$.

To obtain $\boldsymbol{\alpha}$, we need to calculate $\tilde{\boldsymbol{\alpha}}^{(k)}$ via (16) and project $\tilde{\boldsymbol{\alpha}}$ towards the feasibility set of (14). Calculating $\tilde{\boldsymbol{\alpha}}^{(k)}$ requires determining the complex gradients of $f_i(\mathbf{w})$, $i = 1, 2$ with respect to $\mathbf{w}$, i.e., deriving $\nabla f_i(\mathbf{w})$, $i = 1, 2$. The expression of $\nabla f_i(\mathbf{w})$, $i = 1, 2$ can be obtained by the following result.

Lemma 2. *The complex gradient of $f_1(\mathbf{w})$ and $f_2(\mathbf{w})$ respectively take the form given by*

$$\nabla f_1(\mathbf{w}) = [\sigma(\mathbf{h}_1, \mathbf{x}_1)^{\mathrm{T}}, \cdots, \sigma(\mathbf{h}_M, \mathbf{x}_M)^{\mathrm{T}}, \tilde{\sigma}(\mathbf{h}_1, \mathbf{x}_1)^{\mathrm{T}}, \cdots, \tilde{\sigma}(\mathbf{h}_M, \mathbf{x}_M)^{\mathrm{T}}]^{\mathrm{T}} \in \mathbb{C}^{2LM\times 1} \quad (17)$$

and

$$\nabla f_2(\mathbf{w}) = (\tilde{\mathbf{u}}\otimes\mathbf{s})\odot[\sigma(\mathbf{h}_1, \mathbf{q}_1)^{\mathrm{T}}, \cdots, \sigma(\mathbf{h}_M, \mathbf{q}_M)^{\mathrm{T}}, \tilde{\sigma}(\mathbf{h}_1, \mathbf{q}_1)^{\mathrm{T}}, \cdots, \tilde{\sigma}(\mathbf{h}_M, \mathbf{q}_M)^{\mathrm{T}}]^{\mathrm{T}} \in \mathbb{C}^{2LM\times 1} \quad (18)$$

where $\tilde{\mathbf{u}} \triangleq [\mathbf{1}_M^{\mathrm{T}}, \mathbf{0}_M^{\mathrm{T}}]^{\mathrm{T}}$, and $\sigma(\cdot,\cdot)$ and $\tilde{\sigma}(\cdot,\cdot)$ are the operators with two arguments. Without loss of generality, we enforce the definitions given by $\sigma(\mathbf{h}_m, \mathbf{q}_m) \triangleq 2\sum_{l=1-L}^{L-1}\mathbf{S}_l\mathbf{h}_m\mathbf{h}_m^{\mathrm{H}}\mathbf{S}_l^{\mathrm{H}}\mathbf{q}_m + 2(\gamma_1 - 1)\mathbf{h}_m\mathbf{h}_m^{\mathrm{H}}\mathbf{q}_m - 2\gamma_1 c_1\mathbf{h}_m$ and $\tilde{\sigma}(\mathbf{h}_m, \mathbf{q}_m) \triangleq 2\sum_{l=1-L}^{L-1}\mathbf{S}_l^{\mathrm{H}}\mathbf{q}_m\mathbf{q}_m^{\mathrm{H}}\mathbf{S}_l\mathbf{h}_m + 2(\gamma_1 - 1)\mathbf{q}_m\mathbf{q}_m^{\mathrm{H}}\mathbf{h}_m - 2\gamma_1 c_1\mathbf{q}_m$ for $m = 1, \cdots, M$.

Proof. We expand $f_1(\mathbf{w})$ via (5) as the form given by

$$f_1(\mathbf{w}) = \sum_{m=1}^{M}\sum_{l=1-L}^{L-1}\mathbf{x}_m^{\mathrm{H}}\mathbf{S}_l\mathbf{h}_m\mathbf{h}_m^{\mathrm{H}}\mathbf{S}_l^{\mathrm{H}}\mathbf{x}_m + (\gamma_1 - 1) \times \sum_{m=1}^{M}\mathbf{x}_m^{\mathrm{H}}\mathbf{h}_m\mathbf{h}_m^{\mathrm{H}}\mathbf{x}_m - \gamma_1 c_1\sum_{m=1}^{M}(\mathbf{x}_m^{\mathrm{H}}\mathbf{h}_m - \mathbf{h}_m^{\mathrm{H}}\mathbf{x}_m). \quad (19)$$

Based on (19), we express the complex gradient of $f_1(\mathbf{w})$ with respect to $\mathbf{x}_m$ (denoted as $\nabla_{\mathbf{x}_m} f_1(\mathbf{w})$) into the form as

$$\nabla_{\mathbf{x}_m} f_1(\mathbf{w}) = 2 \sum_{l=1-L}^{L-1} \mathbf{S}_l \mathbf{h}_m \mathbf{h}_m^{\mathrm{H}} \mathbf{S}_l^{\mathrm{H}} \mathbf{x}_m + 2(\gamma_1 - 1) \times \mathbf{h}_m \mathbf{h}_m^{\mathrm{H}} \mathbf{x}_m - 2\gamma_1 c_1 \mathbf{h}_m \quad (20)$$

which is obtained via using the fact that the complex gradients of items $\mathbf{g}^{\mathrm{H}}\mathbf{A}\mathbf{g}$, $\mathbf{g}^{\mathrm{H}}\mathbf{f}$, and $\mathbf{f}^{\mathrm{H}}\mathbf{g}$ with respect to $\mathbf{g} \in \mathbb{C}^{L\times 1}$ are respectively $\mathbf{A}\mathbf{g}$, $\mathbf{f}$, and $\mathbf{0}_L$ and enforcing $\mathbf{g} \triangleq \mathbf{x}_m$, $\mathbf{A} \triangleq \sum_{l=1-L}^{L-1} \mathbf{S}_l \mathbf{h}_m \mathbf{h}_m^{\mathrm{H}} \mathbf{S}_l^{\mathrm{H}}$, and $\mathbf{f} \triangleq \mathbf{h}_m$. Using the same routine as used for obtaining (20), we express the complex gradient of $f_1(\mathbf{w})$ with respect to $\mathbf{h}_m$ (denoted as $\nabla_{\mathbf{h}_m} f_1(\mathbf{w})$) as

$$\nabla_{\mathbf{h}_m} f_1(\mathbf{w}) = 2 \sum_{l=1-L}^{L-1} \sum_{l=1-L}^{L-1} \mathbf{S}_l^{\mathrm{H}} \mathbf{x}_m \mathbf{x}_m^{\mathrm{H}} \mathbf{S}_l \mathbf{h}_m + 2(\gamma_1 - 1) \times \mathbf{x}_m \mathbf{x}_m^{\mathrm{H}} \mathbf{h}_m - 2\gamma_1 c_1 \mathbf{x}_m. \quad (21)$$

Substituting (20) and (21) into the fact that $\nabla f_1(\mathbf{w}) = [\nabla_{\mathbf{x}_1} f_1(\mathbf{w})^{\mathrm{T}}, \cdots, \nabla_{\mathbf{x}_M} f_1(\mathbf{w})^{\mathrm{T}}, \nabla_{\mathbf{h}_1} f_1(\mathbf{w})^{\mathrm{T}}, \cdots, \nabla_{\mathbf{h}_M} f_1(\mathbf{w})^{\mathrm{T}}]^{\mathrm{T}}$, the expression of $\nabla f_1(\mathbf{w})$ has the same form as (17).

Similarly, replacing $\mathbf{x}_m$ with $\mathbf{q}_m$, after some straightforward derivations, the expression of $\nabla f_2(\mathbf{w})$ has the same form as (18). The proof is complete. □

Then, we project $\tilde{\boldsymbol{\alpha}}$ calculated by (16) towards the feasibility set of (14), and the adaptive coefficient vector at the k-th iteration can be updated by

$$\boldsymbol{\alpha}^{(k)} = \underset{\substack{\mathbf{1}_2^{\mathrm{T}}\hat{\boldsymbol{\alpha}} \\ \mathbf{1}_2 \succeq \hat{\boldsymbol{\alpha}} \succeq \mathbf{0}_2}}{\operatorname{argmin}} \|\hat{\boldsymbol{\alpha}} - \tilde{\boldsymbol{\alpha}}^{(k)}\|^2 \quad (22)$$

which is an non-negative least squares problem and can be directly solved the 'lsqlin' function in matlab.

B. Multiple-Gradient Descent Based Solution and Projection Toward Constraints

The multiple-gradient descent based update on the reduction of the objective function of (13), associated with $\boldsymbol{\alpha}^{(k)}$ at the k-th iteration, can be expressed as

$$\mathbf{w}^{(k)} = \mathbf{w}^{(k-1)} - 1/\eta^{(k)} \nabla \tilde{f}(\mathbf{w})|_{\mathbf{w}=\mathbf{w}^{(k-1)}} \quad (23)$$

where $\eta^{(k)}$ serves as a adaptive step size for the complex gradient descent based update, and $\nabla \tilde{f}(\mathbf{w})|_{\mathbf{w}=\mathbf{w}^{(k-1)}} = (\hat{\mathbf{W}}^{(k-1)})^{\mathrm{H}} \boldsymbol{\alpha}^{(k)}$. In general, a proper $\eta^{(k)}$ is desired to guarantee the descent of both $f_1(\mathbf{w})$ and $f_2(\mathbf{w})$, but it is difficult to obtain directly. To solve this problem, we can adopt many methods, for example, the multi-objective linear search method (using a modified Armijo's rule) in [16].

After obtaining the gradient descent based solution to minimize (13) by (23), the following task is to conduct proper projections toward the constraints of (13). For the constraints in the unimodular joint design, we just need to manipulate the magnitudes of variable $\mathbf{w}$ to project towards the corresponding feasibility sets. Technically, the projection scheme is given by

$$\mathbf{w}^{(k)} \leftarrow : \sum_{m=1}^{M} \left(\sqrt{\frac{\tilde{L}}{\|\mathbf{w}^{(k)} \odot \mathbf{u}_{m+M}\|}} (\mathbf{w}^{(k)} \odot \mathbf{u}_{m+M}) + \frac{\mathbf{w}^{(k)} \odot \mathbf{u}_m}{|\mathbf{w}^{(k)} \odot \mathbf{u}_m|} \right) \quad (24)$$

where $\mathbf{u}_m \triangleq \mathbf{U}_m^{\mathrm{T}} \mathbf{1}_L \in \mathbb{Z}^{2LM\times 1}$.

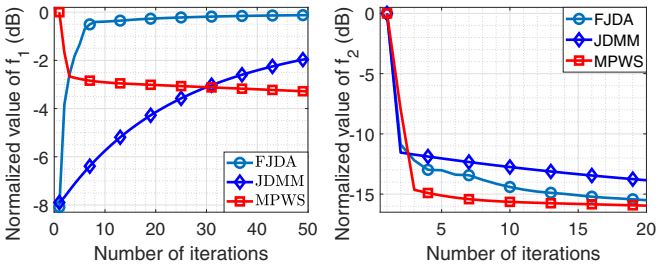

(a) Convergence speed: f_1 case. (b) Convergence speed: f_2 case.

Fig. 1: Objective values versus number of iterations.

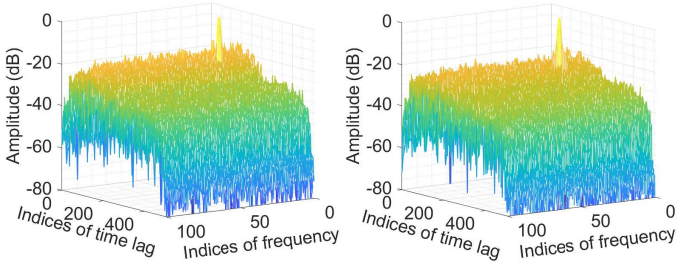

(a) Anti-jamming evaluation of FJDA. (b) Anti-jamming evaluation of MPWS.

Fig. 2: Target detection results of FJDA and MPWS.

IV. Simulations

In our simulations, we evaluate the performance of the proposed algorithm (named hereafter as MPWS) and compare it with that of FJDA algorithm in [10] and the algorithm in [9] (named hereafter as JDMM). Throughout simulations, we generate random sequences as initializations and use the same for each comparison. Moreover, we apply FFT to the compared algorithms if they allow for fast implementations, and use the same acceleration scheme SQUAREM [17] except for JDMM. The stopping criterion ϵ is chosen as the absolute difference between two variables updated at neighboring iterations, which is defined as $\epsilon \triangleq \|\mathbf{w}^{(k)} - \mathbf{w}^{(k-1)}\|^2$. In every example, the repetition interval of sampling is $T = 16\ \mu s$, and the ISRJ sampling duration is $\tau = 2\ \mu s$. Additionally, the objective values shown in dBs are calculated by the operator $20\lg 10(\cdot)$.

Example 1: Convergence evaluation. In this example, we study the convergence properties of FJDA, JDMM, and MPWS in terms of the bi-objective values plotted versus the number of conducted iterations. The values of f_1 and f_2 at each iteration are normalized by the value obtained at initialization. The code length of $L = 64$ is tested, and the number of waveform is set as $M = 1$. The stopping tolerance is 10^{-5}, and the Pareto weight of FJDA is set as 0.8. Other parameters used are: $\gamma_1 = 10$, $\gamma_2 = 500$, $c_1 = 53.849$, $\delta = 60$, $\rho = 0.001$, $c_2 = 0.064$, and $\tilde{L} = 64$.

The corresponding bi-objective convergence results versus the number of conducted iterations are shown in Fig. 1. It can be seen from the figure that MPWS guarantees f_1 and f_2 to decrease simultaneously as the number of iterations increases. However, for FJDA and JDMM, the obtained f_1 increases monotonically as the number of iterations increases. Among the tested algorithms, MPWS shows the best conver-

TABLE I: Comparisons of algorithms versus different code lengths and number of waveforms.

	$M=1,\ L=32$			$M=1,\ L=64$			$M=1,\ L=128$			$M=2,\ L=64$			$M=4,\ L=64$			$M=6,\ L=64$		
	f_1[a]	f_2[b]	DR.[c]	f_1	f_2	DR	f_1	f_2	DR	f_1	f_2	DR	f_1	f_2	DR	f_1	f_2	DR
FJDA	63.91	20.48	36.67%	76.44	31.26	63.33%	89.23	42.33	60%	82.62	37.17	40%	88.50	43.07	40%	92.09	46.66	17.67%
JDMM	66.35	36.73	100%	78.65	46.93	100%	90.81	57.24	100%	-	-	-	-	-	-	-	-	-
MPWS	57.55	27.27	0%	70.47	35.29	0%	84.24	43.45	0%	73.61	48.31	0%	79.29	53.69	3.33%	80.63	57.28	0%

[a] f_1: Average f_1 value (in dB). [b] f_2: Average f_2 value (in dB). [c] DR. : The rate of an algorithm generates the solution dominated by at least one of the other solutions.

gence speed for objective function f_1 and f_2, respectively. This example verifies the advantage of the proposed MPWS algorithm over the other algorithms.

Example 2: Performance evaluation. We evaluate all tested algorithms in terms of the average f_1 value, average f_2 value, and dominated rate (the rate of an algorithm generates the solution dominated by at least one of the other solutions). The set of code lengths $\{32, 64, 128\}$ is used for single waveform design. For multiple waveforms design, the numbers of waveforms are set as $M \in \{2, 4, 6\}$, and the code length is $L = 64$. Other parameters are the same as used in Example 1.

The results of the performance evaluation versus different code lengths and number of waveforms are shown in Table I. It can be seen that the dominated rates of FJDA and JDMM are higher than MPWS for all code lengths. For the comparisons of algorithms versus different number of waveforms, FJDA behaves the worst in terms of the average f_1. For example, the average f_1 value obtained by FJDA is at least 9.01 dB higher than that of MPWS.

Example 3: Anti-jamming performance evaluation. We evaluate the target detection results obtained by MPWS and FJDA in terms of the image of target detection results with the parameters $L = 128$, $M = 100$, $\gamma_1 = 10$, $\gamma_2 = 550$, $c_1 = 83.4230$, $c_2 = 0.0991$, and $\tilde{L} = 76.8$. The carrier frequency is 1000 MHz, duty Ratio is $1/3$, the pulse width is $16\ \mu s$, the sampling frequency is 8 MHz, the target is located at the point $(21, 192)$, and the time delay of jamming is 30 indices. Here, the Pareto weight of FJDA is set as 0.9. Other parameters are the same as used in the last example.

The corresponding results are shown in Fig. 2. It can be seen from the figure that all tested algorithms obtains true target while the false target is suppressed. The normalized jamming peak level, defined as the maximum level except for the true targets in the image results, is suppressed by all tested algorithms. The normalized jamming peak level of FJDA is higher than that of MPWS, reaching at -11.76 dB while those of MPWS is -15.48 dB. This example verifies the advantage of the proposed MPWS algorithm over FJDA.

V. Conclusion

We have proposed a joint design of waveform and mismatched filter to ensure good target detection and anti-jamming performances. Specifically, we employ the weighted sum of the ISL and an SNRL-related penalty term as the primary metric for target detection and the weighted sum of the jamming integrated level and jamming peak level for jamming suppression. This design is formulated into a generalized non-convex bi-objective optimization problem with unimodular constraints and energy restrictions. To solve it, we propose an algorithm based on weighted objectives approach, which involves dynamically determining adaptive weighting coefficients at each iteration and solving the reformulated problem using a multiple-gradient descent based approach. Then, we use projections scheme to address the constraints. Simulations verify the effectiveness of our design.

References

[1] M. Soumekh, "SAR-ECCM using phase-perturbed LFM chirp signals and DRFM repeat jammer penalization," *IEEE Trans. Aerosp. Electron. Syst.*, vol. 42, no. 1, pp. 191–205, Jan. 2006.

[2] N. Li and Y. Zhang, "A survey of radar ECM and ECCM," *IEEE Trans. Aerosp. Electron. Syst.*, vol. 31, no. 3, pp. 1110–1120, Jul. 1995.

[3] Y. Zhang, Y. Wei, and L. Yu, "ISRJ rejection with MIMO radar using space–time complex modulation in multijamming scenario," *IEEE Trans. Aerosp. Electron. Syst.*, vol. 59, no. 6, pp. 8725–8742, Dec. 2023.

[4] J. Akhtar, "Orthogonal block coded ECCM schemes against repeat radar jammers," *IEEE Trans. Aerosp. Electron. Syst.*, vol. 45, no. 3, pp. 1218–1226, Jul. 2009.

[5] S. D. Berger, "Digital radio frequency memory linear range gate stealer spectrum," *IEEE Trans. Aerosp. Electron. Syst.*, vol. 39, no. 2, pp. 725–735, Apr. 2003.

[6] Z. Liu, Y. Quan, S. Du, Y. Wu, M. Sha, and M. Xing, "A novel ECCM scheme against interrupted-sampling repeater jamming using intra-pulse dual-parameter agile waveform," *Digital Signal Processing*, vol. 129, pp. 103652, Sep. 2022.

[7] S. Gong, X. Wei, and X. Li, "ECCM scheme against interrupted sampling repeater jammer based on time-frequency analysis," *Journal of Systems Engineering and Electronics*, vol. 25, no. 6, pp. 996–1003, Dec. 2014.

[8] W. Wu, J. Zou, J. Chen, S. Xu, and Z. Chen, "False-target recognition against interrupted-sampling repeater jamming based on integration decomposition," *IEEE Trans. Aerosp. Electron. Syst.*, vol. 57, no. 5, pp. 2979–2991, Oct. 2021.

[9] K. Zhou, D. Li, S. Quan, T. Liu, Y. Su, and F. He, "SAR waveform and mismatched filter design for countering interrupted-sampling repeater jamming," *IEEE Trans. Geosci. Remote Sens.*, vol. 60, pp. 1–14, Sep. 2022.

[10] K. Zhou, Y. Su, D. Wang, H. Ma, L. Liu, and C. Li, "Improved SAR interrupted-sampling repeater jamming countermeasure based on waveform agility and mismatched filter design," *IEEE Trans. Geosci. Remote Sens.*, vol. 61, pp. 1–16, Apr. 2023.

[11] Y. Gao, H. Fan, L. Ren, Z. Liu, Q. Liu, and E. Mao, "Joint design of waveform and mismatched filter for interrupted sampling repeater jamming suppression," *IEEE Trans. Aerosp. Electron. Syst.*, vol. 59, no. 6, pp. 8037–8050, Jul. 2023.

[12] F. Wang, N. Li, C. Pang, C. Li, Y. Li, and X. Wang, "Complementary sequences and receiving filters design for suppressing interrupted sampling repeater jamming," *IEEE Geosci. Remote Sens. Lett.*, vol. 19, pp. 1–5, Mar. 2022.

[13] X. Lin, Hong. Chen, Chang. Pei, F. Sun, X. Xiao, H. Sun, Y. Zhang, W. Ou, and P. Jiang, "A pareto-efficient algorithm for multiple objective optimization in e-commerce recommendation," *Proceedings of the 13th ACM Conference on Recommender Systems*, Sep. 2019.

[14] A. Bos, "Complex gradient and hessian," Dec., vol. 141, pp. 380–383.

[15] J.-A. Désidéri, "Multiple-gradient descent algorithm (MGDA) for multiobjective optimization," *Comptes Rendus Mathematique*, vol. 350, no. 5, pp. 313–318, Mar. 2012.

[16] A. Tougma, S. Kounhinir, and A. Compaore, "Extension of the projected gradient and Armijo's Rule concepts for solving convex nonlinear multiobjective optimization problems," *Research Square*, Jan. 2023.

[17] J. Song, P. Babu, and D. P. Palomar, "Sequence set design with good correlations properties via Majorization-Mimimization," *IEEE Trans. Signal Process.*, vol. 64, no. 11, pp. 2866–2879, June 2016.